Heterogeneous Catalysis

International Edition: DOI: 10.1002/anie.201703669
German Edition: DOI: 10.1002/ange.201703669

Directing Reaction Pathways through Controlled Reactant Binding at Pd–TiO_2 Interfaces

Jing Zhang[+], Bingwen Wang[+], Eranda Nikolla, and J. Will Medlin**

Abstract: *Recent efforts to design selective catalysts for multi-step reactions, such as hydrodeoxygenation (HDO), have emphasized the preparation of active sites at the interface between two materials having different properties. However, achieving precise control over interfacial properties, and thus reaction selectivity, has remained a challenge. Here, we encapsulated Pd nanoparticles (NPs) with TiO_2 films of regulated porosity to gain a new level of control over catalyst performance, resulting in essentially 100 % HDO selectivity for two biomass-derived alcohols. This catalyst also showed exceptional reaction specificity in HDO of furfural and m-cresol. In addition to improving HDO activity by maximizing the interfacial contact between the metal and metal oxide sites, encapsulation by the nanoporous oxide film provided a significant selectivity boost by restricting the accessible conformations of aromatics on the surface.*

Interfacial sites between metals and metal oxides have been proposed to be important in many catalytic reactions.[1] Such interfaces can form the basis of bifunctional catalysis, where each material contributes its unique functionality to the active site. For example, bifunctional catalysts have shown promise for selective hydrodeoxygenation (HDO) of alcohols/aldehydes with aromatic substituents, a desirable path for production of fuels or chemicals from biomass (Figure 1 a).[1–3] While the mechanism for interfacial reactivity is under debate, reducible metal oxides (e.g. TiO_2, CeO_2) have been suggested to provide deoxygenation sites, while the noble metals (e.g, Pd, Ru) provide hydrogenation sites.[4–8]

The importance of interfacial sites in catalysis suggests that catalyst design should emphasize novel methods for tailoring these interfaces that go beyond using the oxide as a simple catalyst carrier.[9,10] A promising approach is to employ inverted systems in which the metal oxide is deposited as a film onto the metal nanoparticles (NPs). While encapsulated structures have been applied to enhance the stability of metal NPs[11–14] or improve the selectivity and/or activity for selective oxidation,[15–17] hydrogenation,[18–20] and decarbonylation,[21] HDO provides an important probe reaction for testing their utility for reactions that occur at metal/oxide interfaces. Moreover, the unique geometry of the sites in an encapsulated structure could result in a new way to control interfacial properties via biasing the reactant binding orientations. For aromatic alcohols, flat-lying adsorbates are prone to decarbonylation and ring hydrogenation while upright adsorption geometries favor HDO.[22–28] Here, we report on a method for controlling the encapsulation of Pd NPs with nanoporous TiO_2 to produce interfacial sites where accessible conformations of aromatics are restricted. The resulting catalysts exhibited high selectivity toward HDO with

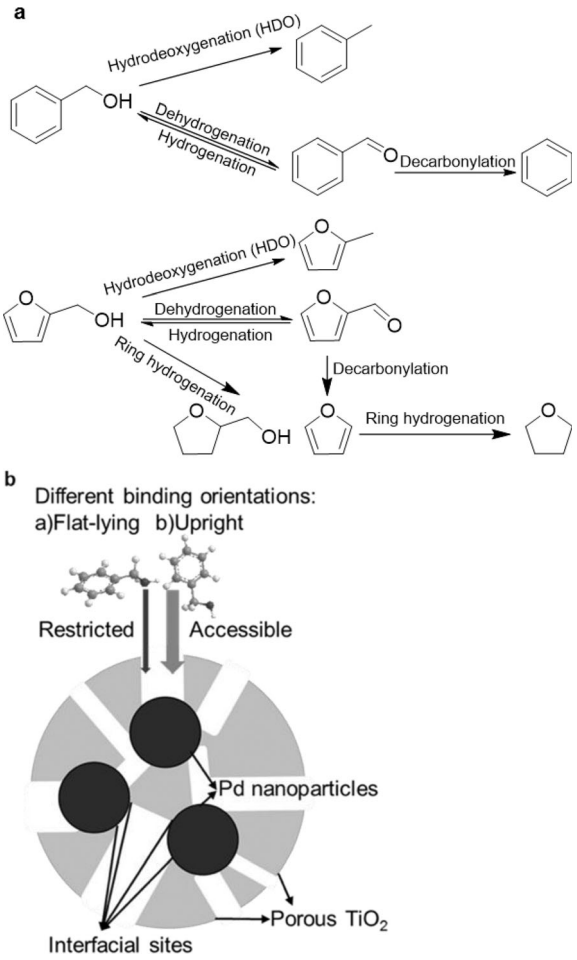

Figure 1. a) Reaction pathways of benzyl alcohol and furfuryl alcohol on Pd catalysts. b) Controlled binding as well as interfacial sites induced by nanoporous TiO_2 film.

[*] Dr. J. Zhang,[+] Prof. Dr. J. W. Medlin
Department of Chemical and Biological Engineering
University of Colorado Boulder
Boulder, CO 80303 (USA)
E-mail: will.medlin@colorado.edu
B. Wang,[+] Prof. Dr. E. Nikolla
Department of Chemical Engineering and Materials Science
Wayne State University
Detroit, MI 48202 (USA)
E-mail: erandan@wayne.edu
[+] These authors contributed equally to this work.

Supporting information and the ORCID identification number(s) for the author(s) of this article can be found under: https://doi.org/10.1002/anie.201703669.

improved activity during reactions of furfuryl alcohol, benzyl alcohol, furfural and *m*-cresol. The improvements were attributed to a combined effect of controlling binding orientation of the aromatics and the presence of metal–support interfacial sites, as illustrated in Figure 1 b.

Using a method modified based on Klabunde and co-workers,[29] we synthesized Pd^0 particles which were uniform in size ($\approx$4 nm) and well-dispersed in solution, as confirmed by transmission electron microscopy (TEM) and X-ray diffraction (XRD) (Figure S1 in the Supporting Information). Prior to synthesis of TiO_2 films, a layer of surfactant molecules (cetyl trimethylammonium bromide (CTAB)) was deposited on the dispersed Pd NPs. The microstructure of the TiO_2 films was controlled by adjusting the rate of hydrolysis of the titanium precursor via varying the rate of the water addition[30] or lowering the reactivity of the titanium precursor using acetone.[30–32]

Figure 2 a shows the scanning transmission electron micrographs (STEM) along with the bright field TEM (BF-TEM) of the Pd@TiO_2 structure synthesized by instantaneous addition of water during synthesis (Pd@TiO_2-WI). Lattice fringes of anatase TiO_2 (101) are observed on top of the Pd NPs (circled in black) with measured values of 0.318 nm, consistent with the calculated value from the XRD spectrum (Figure S2), confirming that the Pd NPs are encapsulated by the TiO_2 film. Similar STEM and BF-TEM results were obtained for the case when Pd@TiO_2 were synthesized using a dropwise injection rate for water (Pd@TiO_2-WD) and when water was replaced by acetone during synthesis (Pd@TiO_2-AI), as shown in Figure 2 b and c, respectively. Electron energy loss spectroscopy (EELS) measurements (Figure S3) on Pd@TiO_2-WI were also consistent with Pd NPs being surrounded by the TiO_2 film. Narrow troughs in the TiO_2 EELS signal along the line were detected, perhaps due to the porous structure of the film (Figure S3c). The pore size distribution of the Pd@TiO_2 materials showed that most of the pores (82 %) of Pd@TiO_2-WI were less than 5 nm in width with an average pore size of 4.8 nm (Figure 2a3) while the TiO_2 film of Pd@TiO_2-WD had larger pores (ca. 50 % of the pores $>$5 nm in width, Figure 2b3). A further increase in the pore size was observed for Pd@TiO_2-AI, with about 70 % of the pores larger than 15 nm (Figure 2c3). We also synthesized 4 nm Pd NPs supported on pre-synthesized TiO_2 (Pd/TiO_2) and on a commercial α-Al_2O_3 support (Pd/Al_2O_3) by incipient wetness impregnation. The STEM image of the former is shown in Figure 2 d. Unlike the encapsulated systems (Figure 2 a–c), as expected the TiO_2 (101) fringes were only found on the support and not on top of the Pd NPs (circled in black) (Figure 2 d). The Pd NPs were dominated by the Pd (111) lattice fringes, measured to be 0.225 nm, in agreement with the calculated value from the XRD spectrum (Experimental Procedure and Figure S4b in the Supporting Information).

The weight loading and apparent dispersion of Pd was determined by ICP-OES and CO chemisorption, respectively. The results in Table S1 suggest that the active sites for HDO were minimally blocked by the TiO_2 film in all cases, likely due to the high porosity of the film (0.12 $cm^3\,g^{-1}$ for Pd@TiO_2-WI). Table S1 also shows that Pd@TiO_2-WI had the lowest Pd loading, likely due to the fast hydrolysis of the titanium

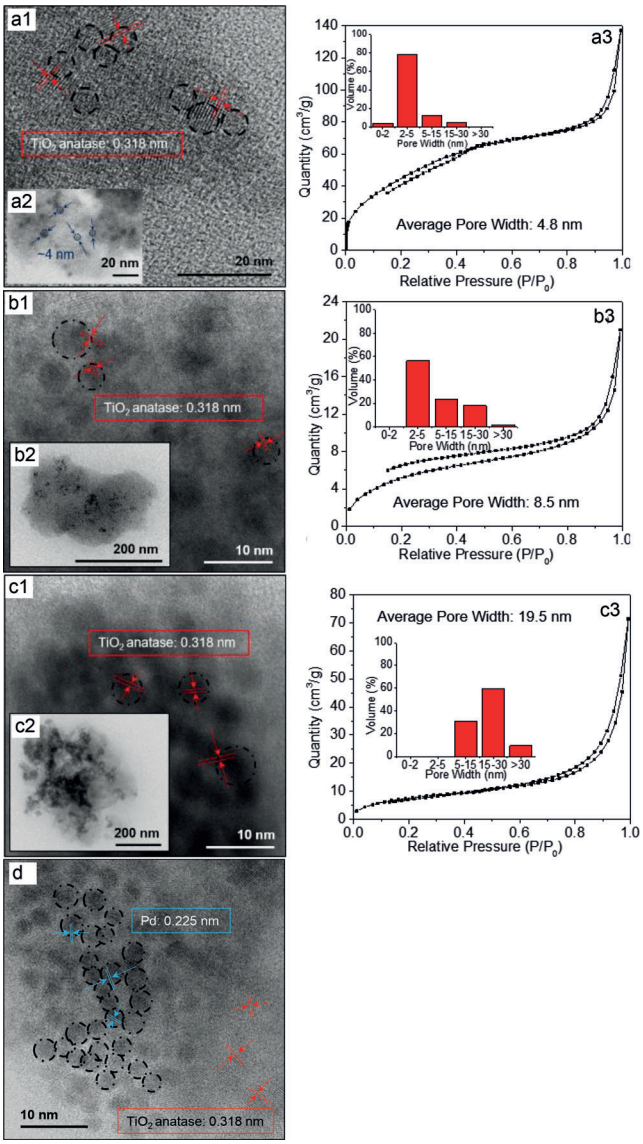

Figure 2. Characterization of a) Pd@TiO_2-WI, b) Pd@TiO_2-WD, c) Pd@TiO_2-AI: 1) STEM images, 2) BF-TEM images, 3) N_2 physisorption isotherm plots and pore size distribution of TiO_2 films on Pd NPs; d) STEM image of Pd/TiO_2.

precursor. Infrared spectra measured after CO adsorption indicated that TiO_2 encapsulation had little effect on the types of Pd sites available for adsorption (Figure S5).

Catalysts were evaluated for benzyl alcohol HDO; the catalyst performance as a function of time on stream is shown in Figure S6 in the Supporting Information. Figure 3 summarizes the effects of support and encapsulation on the catalyst performance. For impregnated Pd NPs, changing the support from Al_2O_3 to TiO_2 led to an increase in HDO selectivity from 36 % to 50 % (Figure 3 a). Encapsulation with TiO_2 further increased the selectivity to 84 and 88 % for Pd@TiO_2-WD and Pd@TiO_2-AI, respectively. For Pd@TiO_2-WI which contained narrower pores, a HDO selectivity of approximately 100 % was obtained. We found that the improved selectivity was not only owed to suppression of the undesired reaction pathways but higher rates for toluene formation (Figure 3 b).

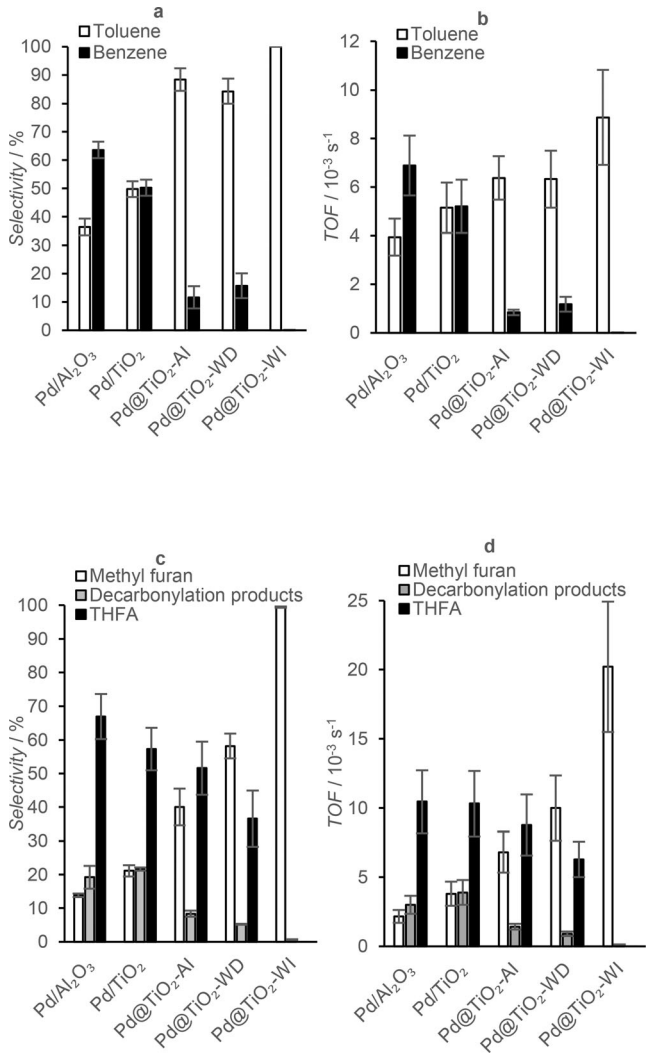

Figure 3. Selectivity and turnover frequency (TOF) for catalytic conversion of benzyl alcohol (a,b) and furfuryl alcohol (c,d). Reaction conditions are shown in Experimental Procedures in the Supporting Information. Decarbonylation products refer to furan and THF.

Catalyst performance was also evaluated for HDO of furfuryl alcohol; the catalyst performance with time on stream is shown in Figure S6 in the Supporting Information. Unlike benzyl alcohol, two ring hydrogenation products, tetrahydrofuran (THF) and tetrahydrofurfuryl alcohol (THFA), were formed from furfuryl alcohol. Similar to the case for benzyl alcohol, encapsulation of the Pd NPs with TiO_2 dramatically improved the selectivity towards HDO (Figure 3c). Furthermore, when the TiO_2 film mainly contained small pores (Pd@TiO_2-WI), HDO became the only observed pathway. The comparison of the turnover frequencies for the different catalysts (Figure 3d) shows that the improved selectivity for the Pd@TiO_2 was again due to both an increase in HDO rate and a decrease in other pathways. Post-reaction characterization using STEM and BF-TEM (Figure S7) showed that unlike the Pd/TiO_2, the Pd@TiO_2-WI retained its particle size and encapsulation structure after reactions.

We conducted kinetic studies to evaluate the effect of the TiO_2 film on activation energies for benzyl alcohol conversion (Figure S8). We found similar activation energies of 90–93 kJ mol^{-1} for benzene formation on all the encapsulated Pd and the supported Pd catalysts, suggesting that the decrease in decarbonylation rate was caused by lower active site density, rather than a change in the mechanism. The apparent activation energy for HDO, however, varied greatly among different catalysts. For Pd@TiO_2-WI, a value of 87 kJ mol^{-1} was measured, which is similar to the ca. 100 kJ mol^{-1} measured on a crowded Pd (111) single crystal.[22,23] For impregnated Pd and encapsulated Pd with larger pores, the apparent activation energy was less than 30 kJ mol^{-1}, which is much lower than a typical C–O dissociation barrier. Low or negative apparent activation energies have frequently been observed for HDO on metal catalysts, and have been attributed to poisoning of active sites by dehydrogenated adsorbates, the effect of which is strong at high temperature.[26,33] Encapsulation of Pd within the smallest-pore TiO_2 structures thus appears to have decreased the effects of these side reactions on the surface chemistry, in line with the high observed HDO selectivity.

We hypothesized that the improved performance of TiO_2-encapsulated Pd as compared to supported catalysts was due to two effects: the larger concentration of Pd-TiO_2 interfacial sites, and the restriction of unfavorable adsorbate binding geometries. It has been reported that using reducible metal oxides as a support could promote HDO since the partially reduced oxide creates oxygen vacancies to facilitate adsorption and C–O activation of hydroxylated reactants.[4–6] The presence of metals capable of hydrogen spillover was found to enhance the reducibility of the metal oxides.[34,35] For example, Prins and co-workers[34] found that for Pt/TiO_2 catalysts, reduction of TiO_2 in the near vicinity of Pt began by 500 K. We performed temperature programmed reduction (TPR) to evaluate the reducibility of the metal oxide supports (note that the Pd NPs were already in a reduced state) for the various catalysts. To limit interference from moisture desorption, deuterium (D_2) was used as reducing gas during the TPR and the signal of D_2 ($m/z = 4$) and D_2O ($m/z = 20$) was recorded to detect reduction. As shown in Figure S9 in the Supporting Information, the onset reduction temperature, represented by a simultaneous decrease in the D_2 signal and increase of the D_2O signal, followed a sequence of Pd@TiO_2 < Pd/TiO_2 < TiO_2, which is consistent with the HDO selectivity and activity for the Pd-containing catalysts (Al_2O_3 is considered non-reducible in this temperature range). Pd@TiO_2 showed the lowest onset reduction temperature of ca. 160 °C; in contrast, consistent with prior work for Pt/TiO_2,[34] the reduction of a conventional TiO_2-supported system began close to 230 °C. These results suggest that intimate contact between Pd and reducible TiO_2 (as achieved in the Pd@TiO_2 materials) is key for HDO performance.

Better reducibility of TiO_2 alone could not explain the 100% selectivity to toluene and 2-methyl furan over Pd@TiO_2-WI, since its TPR profile was similar to Pd@TiO_2-WD (Figure S9). Moreover, the negligible turnover frequency for decarbonylation over Pd@TiO_2-WI (Figure 3c–d) suggests the elimination of sites associated with that reaction. The

classical strong metal-support interaction (SMSI) induced by high temperature reduction could alter the HDO selectivity, but is unlikely in our case since none of the catalysts went through the high temperature reduction necessary to induce the SMSI. We hypothesized that the TiO_2 film consisting mainly of small pores (Pd@TiO_2-WI) discouraged "flat-lying" adsorption of the reactant molecules, while favoring "upright" adsorption. To support this hypothesis, we investigated the hydrogenation of two probe molecules, styrene and 1-hexene, over the catalysts. The planar structure of styrene is expected to occupy a larger collection of contiguous Pd atoms at the catalyst surface, with a similar "footprint" to flat-lying benzyl alcohol and furfuryl alcohol, while the non-aromatic 1-hexene would occupy fewer sites on the surface due to the absence of an aromatic substituent.

The relative rates of the hydrogenation probe reactions are plotted in Figure 4. Pd@TiO_2-WI exhibited a much lower activity for hydrogenation of styrene, while the other encapsulated and supported Pd materials showed comparable activity for this reaction. In contrast, all the Pd catalysts showed similar activities for hydrogenation of 1-hexene. These results suggest a significant restriction for styrene adsorption and hydrogenation on Pd@TiO_2-WI, supporting the hypothesis that suppression of the flat-lying adsorption of the reactant molecules contributes to the high HDO selectivity in the case of Pd@TiO_2-WI, as depicted in Figure 1b.

To further verify how reactants bind to the surface and the resultant product from different binding orientations, we performed isotopic studies using D_2 instead of H_2 for HDO of benzyl alcohol. Figure 5b shows that H/D exchange occurred for all six aromatic H atoms of benzene, which verified benzene formation was likely through a "flat-lying" adsorbate configuration, which enables facile exchange of aromatic H with surface D. To the contrary, aromatic H/D exchange was not observed for toluene (Figure 5a), suggesting its formation

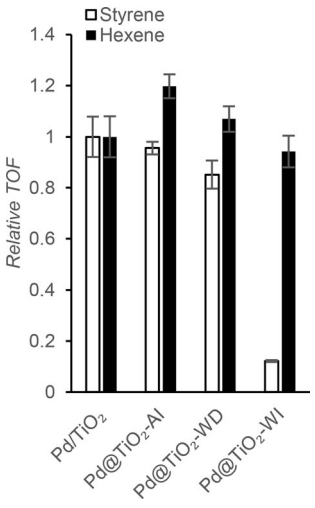

Figure 4. Relative TOF of hydrogenation of olefins with different sizes (styrene and 1-hexene) versus catalytic conversion of benzyl alcohol. Reaction conditions are shown in Experimental Procedures in the Supporting Information. The relative TOF for Pd/TiO_2 was normalized to 1 for both reactions using scaling factors. The same scaling factors were used for all other Pd catalysts to ensure quantitative comparison among them.

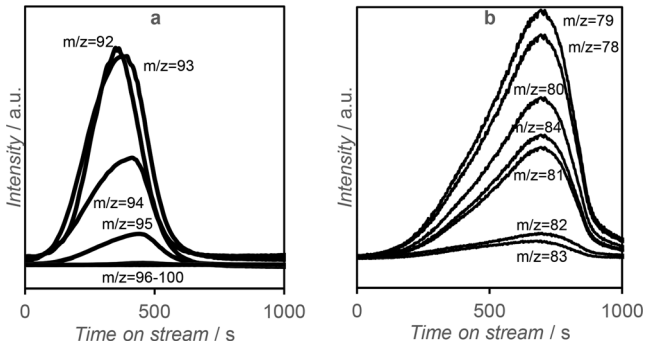

Figure 5. Mass spectra from a pulse of benzyl alcohol over Pd/TiO_2 that was precovered by D_2: a) ions for toluene, b) ions for benzene; conditions: temperature: 190 °C, pressure: 1 atm; mole fraction of the pulse: $Y_{D2} = 20\,\%$, $Y_{\text{benzyl alcohol}} = 0.03\,\%$; gas flow rates: 140 mL min^{-1}.

occurred through a more "upright" adsorption, which only enabled the H/D exchange on the methyl group. No aromatic H/D exchange was observed for Pd@TiO_2-WI, with toluene being the only product (Figure S10), evidencing the restriction of "flat-lying" adsorption on Pd@TiO_2-WI. We also conducted the isotopic study for hydrogenation of styrene (Figure S11), which showed that the H/D exchange occurred for all aromatic H atoms, suggesting its adsorption pattern is also "flat-lying". The similar restriction for both benzene and ethylbenzene formation from benzyl alcohol and styrene, respectively, strongly suggests that the Pd@TiO_2-WI restrained "flat-lying" adsorption of aromatic reactants thereby improving HDO selectivity. We propose two possible mechanisms for the apparent restriction of flat-lying adsorption. First, the confined pores of TiO_2 films on Pd@TiO_2-WI may provide a more crowded surface to disrupt contiguous arrays of active sites ("ensembles") necessary for flat-lying adsorption. It should be noted that the detailed connection between bulk pore size and the structure of available sites around the interface is not clear; the results reported here suggest that the surface crowding on Pd@TiO_2-WI may be more severe than would be expected based on the average (bulk) pore size. Alternatively, chemical interactions between TiO_x and Pd may contribute to the selectivity boost for Pd@TiO_2-WI, for example via more extensive electronic perturbation of Pd sites within more highly confined pores.

To investigate the generality of this approach, the Pd catalysts were used for HDO of furfural and *m*-cresol to produce 2-methyl furan and toluene, respectively. For these reactions, noble metals suffer poor reaction specificity despite their high activity/stability; alloys and base metals have been considered as substitutes.[36–38] As with the model reactants, we observed high HDO selectivity using the Pd@TiO_2-WI (Figure 6). Figure S12 shows that the improved selectivity was due to faster HDO rates and suppression of decarbonylation and ring hydrogenation. It may be interesting to use a similar encapsulation approach to enhance properties of more inherently selective alloy and base metal catalysts.

In conclusion, we showed that the HDO selectivity of aromatic alcohols/aldehydes and phenolics can be significantly enhanced by encapsulating Pd NPs with porous TiO_2, while maintaining high catalytic activity. While all the

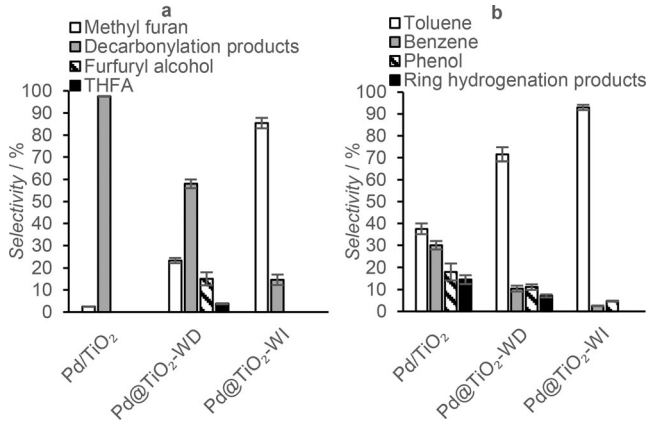

Figure 6. Selectivity for catalytic conversion of a) furfural and b) *m*-cresol; decarbonylation products refer to furan and THF, ring hydrogenation products refer to 3-methylcyclohexane and 3-methylcyclohexanone. Reaction conditions are shown in Experimental Procedures in the Supporting Information.

$Pd@TiO_2$ materials showed enhanced performance due to the extent of interaction between the metal and metal oxide, TiO_2 films with confined porosity led to the highest HDO selectivity, which was mainly attributed to favorable adsorption orientations of the aromatics on the active sites. These results indicate that encapsulated NPs may be useful both in generating unique types of interfacial sites and in controlling how reactant molecules coordinate to them.

Acknowledgements

The authors acknowledge support from the National Science Foundation for funding this research through DMREF Grant #1436206.

Conflict of interest

The authors declare no conflict of interest.

Keywords: biomass-derived alcohols · encapsulation · heterogeneous catalysis · hydrodeoxygenation · nanoparticles

[1] A. M. Robinson, J. E. Hensley, J. W. Medlin, *ACS Catal.* **2016**, *6*, 5026.
[2] D. D. Laskar, B. Yang, H. Wang, J. Lee, *Biofuels Bioprod. Biorefin.* **2013**, *7*, 602.
[3] M. Besson, P. Gallezot, C. Pinel, *Chem. Rev.* **2014**, *114*, 1827.
[4] A. Saadi, R. Merabti, Z. Rassoul, M. M. Bettahar, *J. Mol. Catal. A* **2006**, *253*, 79.
[5] P. M. De Souza, R. C. Rabelo-Neto, L. E. P. Borges, G. Jacobs, B. H. Davis, T. Sooknoi, D. E. Resasco, F. B. Noronha, *ACS Catal.* **2015**, *5*, 1318.
[6] P. M. De Souza, L. Nie, L. E. P. Borges, F. B. Noronha, D. E. Resasco, *Catal. Lett.* **2014**, *144*, 2005.
[7] T. Omotoso, S. Boonyasuwat, S. P. Crossley, *Green Chem.* **2014**, *16*, 645.
[8] R. C. Nelson, B. Baek, P. Ruiz, B. Goundie, A. Brooks, M. C. Wheeler, B. G. Frederick, L. C. Grabow, R. N. Austin, *ACS Catal.* **2015**, *5*, 6509.
[9] W. Song, C. Zhao, J. A. Lercher, *Chem. Eur. J.* **2013**, *19*, 9833.
[10] B. Qiao, A. Wang, X. Yang, L. F. Allard, Z. Jiang, Y. Cui, J. Liu, J. Li, T. Zhang, *Nat. Chem.* **2011**, *3*, 634.
[11] G. D. Li, Z. Y. Tang, *Nanoscale* **2014**, *6*, 3995.
[12] Q. Zhang, I. Lee, J. B. Joo, F. Zaera, Y. Yin, *Acc. Chem. Res.* **2013**, *46*, 1816.
[13] H. C. Zeng, *Acc. Chem. Res.* **2013**, *46*, 226.
[14] L. Liu, U. Díaz, R. Arenal, G. Agostini, P. Concepción, A. Corma, *Nat. Mater.* **2016**, *16*, 132.
[15] Q. Fu, W.-X. Li, Y. Yao, H. Liu, H.-Y. Su, D. Ma, X.-K. Gu, L. Chen, Z. Wang, H. Zhang, B. Wang, X. Bao, *Science* **2010**, *328*, 1141.
[16] J. Qi, J. Chen, G. Li, S. Li, Y. Gao, Z. Tang, *Energy Environ. Sci.* **2012**, *5*, 8937.
[17] H. Hong, L. Hu, M. Li, J. Zheng, X. Sun, X. Lu, X. Cao, J. Lu, H. Gu, *Chem. Eur. J.* **2011**, *17*, 8726.
[18] T. Mitsudome, Y. Mikami, M. Matoba, T. Mizugaki, K. Jitsukawa, K. Kaneda, *Angew. Chem. Int. Ed.* **2012**, *51*, 136; *Angew. Chem.* **2012**, *124*, 140.
[19] T. Mitsudome, M. Matoba, T. Mizugaki, K. Jitsukawa, K. Kaneda, *Chem. Eur. J.* **2013**, *19*, 5255.
[20] M. Zhao, K. Yuan, Y. Wang, G. Li, J. Guo, L. Gu, W. Hu, H. Zhao, Z. Tang, *Nature* **2016**, *539*, 76.
[21] C. Wang, L. Wang, J. Zhang, H. Wang, J. P. Lewis, F. S. Xiao, *J. Am. Chem. Soc.* **2016**, *138*, 7880.
[22] S. H. Pang, A. M. Román, J. W. Medlin, *J. Phys. Chem. C* **2012**, *116*, 13654.
[23] C. H. Lien, J. W. Medlin, *J. Phys. Chem. C* **2014**, *118*, 23783.
[24] S. H. Pang, J. W. Medlin, *ACS Catal.* **2011**, *1*, 1272.
[25] G. Kumar, C.-H. Lien, M. J. Janik, J. W. Medlin, *ACS Catal.* **2016**, *6*, 5086.
[26] C. H. Lien, J. W. Medlin, *J. Catal.* **2016**, *339*, 38.
[27] V. Vorotnikov, G. Mpourmpakis, D. G. Vlachos, *ACS Catal.* **2012**, *2*, 2496.
[28] S. H. Pang, C. A. Schoenbaum, D. K. Schwartz, J. W. Medlin, *Nat. Commun.* **2013**, *4*, 2448.
[29] Z. Q. Yang, K. J. Klabunde, *J. Organomet. Chem.* **2009**, *694*, 1016.
[30] M. Niederberger, *Met. Oxide Nanoparticles Org. Solvents* **2009**, 7.
[31] N. Steunou, F. Ribot, K. Boubekeur, J. Maquet, C. Sanchez, *New J. Chem.* **1999**, *23*, 1079.
[32] G. Garnweitner, M. Antonietti, M. Niederberger, *Chem. Commun.* **2005**, 397.
[33] N. Singh, Y. Song, O. Y. Gutiérrez, D. M. Camaioni, C. T. Campbell, J. A. Lercher, *ACS Catal.* **2016**, *6*, 7466.
[34] T. Huizinga, J. Van Grondelle, R. Prins, *Appl. Catal.* **1984**, *10*, 199.
[35] A. J. R. Hensley, Y. Hong, R. Zhang, H. Zhang, J. Sun, Y. Wang, J. S. McEwen, *ACS Catal.* **2014**, *4*, 3381.
[36] S. H. Pang, N. E. Love, J. W. Medlin, *J. Phys. Chem. Lett.* **2014**, *5*, 4110.
[37] A. M. Robinson, G. A. Ferguson, J. R. Gallagher, S. Cheah, G. T. Beckham, J. A. Schaidle, J. E. Hensley, J. W. Medlin, *ACS Catal.* **2016**, *6*, 4356.
[38] L. Nie, P. M. Souza, F. B. Noronha, W. An, T. Sooknoi, D. E. Resasco, *J. Mol. Catal. A* **2014**, *388*, 47.

Manuscript received: April 9, 2017
Final Article published: ■■ ■■, ■■■■

Communications

Heterogeneous Catalysis

J. Zhang, B. Wang, E. Nikolla,*
J. W. Medlin* _____ ■■■■–■■■■

Directing Reaction Pathways through Controlled Reactant Binding at Pd–TiO_2 Interfaces

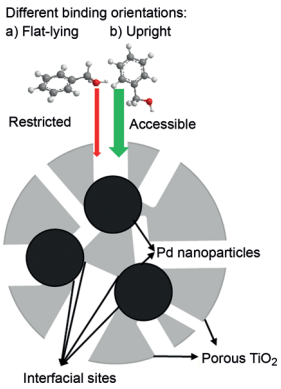

Nanoscale morphology control over active sites consisting of Pd and TiO_2 specifies binding orientation of reactant molecules to provide unprecedented reaction specificity toward hydrodeoxygenation during catalytic conversion of biomass-derived aromatic alcohols/aldehydes and phenolics.